PAPER

Effect of annealing in oxygen on alloy structures of Pd–Au bimetallic model catalysts†

Wen-Yueh Yu,[a] Liang Zhang,[bc] Gregory M. Mullen,[a] Edward J. Evans Jr.,[b] Graeme Henkelman[bc] and C. Buddie Mullins*[abd]

It has been reported that Pd–Au bimetallic catalysts display improved catalytic performance after adequate calcination. In this study, a model catalyst study was conducted to investigate the effects of annealing in oxygen on the surface structures of Pd–Au alloys by comparing the physicochemical properties of Pd/Au(111) surfaces that were annealed in ultrahigh vacuum (UHV) *versus* in an oxygen ambient. Auger electron spectroscopy (AES) and Basin hopping simulations reveal that the presence of oxygen can inhibit the diffusion of surface Pd atoms into the subsurface of the Au(111) sample. Reflection–absorption infrared spectroscopy using CO as a probe molecule (CO-RAIRS) and King–Wells measurements of O_2 uptake suggest that surfaces annealed in an oxygen ambient possess more contiguous Pd sites than surfaces annealed under UHV conditions. The oxygen-annealed Pd/Au(111) surface exhibited a higher activity for CO oxidation in reactive molecular beam scattering (RMBS) experiments. This enhanced activity likely results from the higher oxygen uptake and relatively facile dissociation of oxygen admolecules due to stronger adsorbate–surface interactions as suggested by temperature-programmed desorption (TPD) measurements. These observations provide fundamental insights into the surface phenomena of Pd–Au alloys, which may prove beneficial in the design of future Pd–Au catalysts.

1. Introduction

Bimetallic catalysts have received substantial attention as their physicochemical properties often differ from those of their parent metals, which hold the promise of enhanced activity, selectivity and stability.[1,2] As one of the most studied bimetallic systems, Pd–Au catalysts have displayed promising performance for a broad range of catalytic reactions such as CO oxidation,[3–5] acetoxylation of ethylene to vinyl acetate,[6,7] selective oxidation of alcohols,[8–11] selective hydrogenation of unsaturated hydrocarbons,[12–15] hydrodechlorination of chlorinated compounds,[16–18] hydrodesulfurization of sulfur-containing molecules,[19,20] decomposition of liquid hydrocarbons for H_2 production,[21,22] and the direct synthesis of H_2O_2 from H_2 and O_2.[23–28] It has been suggested that the synergistic effects observed for Pd–Au bimetallic catalysts originate from the formation of alloy structures (homogeneous or core–shell) that electronically modify the nature of the active sites.[11,20,28]

Recently, it was reported that adequate calcination (*i.e.*, annealing in air) can efficiently improve the catalytic performance of Pd–Au catalysts.[5,20,25–29] Scanning transmission electron microscopy (STEM) imaging showed that calcination can modify the alloy structure of Pd–Au nanoparticles.[25–29] The evolution of the alloy structure upon calcination appears to be a complex process as it depends on the calcination temperature,[25–29] type of support material used,[25–28] and method of catalyst preparation.[27,28] For instance, with TiO_2 as the support material, Pd–Au nanoparticles changed from a Pd-rich shell and Au-rich core structure to a homogeneous alloy when the calcination temperature was increased from 350 to 700 °C.[29] The structure of Pd–Au nanoparticles immobilized on carbon remained as a homogeneous alloy after calcination at 450 °C, whereas TiO_2- and Al_2O_3-supported Pd–Au nanoparticles transformed into a Pd-rich shell and Au-rich core structure.[25]

A molecular-level investigation of how the structure and composition of Pd–Au surfaces change in response to annealing in an oxygen ambient could enhance the fundamental understanding of the calcination effect on Pd–Au catalysts. In model catalyst studies, well-defined single-crystal surfaces are prepared under UHV conditions and characterized *in situ* by surface science techniques, which enable surface characterization at the molecular level with minimal environmental interference.[1,2,30–35]

[a] McKetta Department of Chemical Engineering, University of Texas at Austin, Austin, Texas 78712, USA. E-mail: mullins@che.utexas.edu

[b] Department of Chemistry, University of Texas at Austin, Austin, Texas 78712, USA

[c] Institute for Computational Engineering and Sciences, University of Texas at Austin, Austin, Texas 78712, USA

[d] Center for Nano and Molecular Science and Technology, Texas Materials Institute, Center for Electrochemistry, University of Texas at Austin, Austin, Texas 78712, USA

† Electronic supplementary information (ESI) available. See DOI: 10.1039/c5cp03515e

The evolution of the surface structure and composition of Pd–Au model catalysts upon annealing in UHV has been extensively studied.[36–49] For example, using low-energy ion-scattering spectroscopy (LEISS), Koel *et al.*[36] showed that annealing in UHV causes the diffusion of surface Pd atoms into the subsurface of the Au(111) single-crystal (*i.e.*, alloying) at temperatures as low as 240 K. On the other hand, the intermixing of Au with Pd occurred at much higher temperatures ($>$600 K) for an Au overlayer on the Pd(111) surface.[41,45] In contrast to extensive studies of annealing under UHV conditions, very little attention has been paid to experimental investigations with annealing Pd–Au model catalysts in an oxygen ambient. Recently, the influence of adsorbed oxygen on the segregation of a Pd monomer in the Au(111) surface was studied theoretically.[50,51] By using density functional theory (DFT) analyses, Guesmi and co-workers[50] demonstrated that when oxygen atoms are present on the surface, the Pd monomer is energetically more favorable at the topmost layer of Au(111) surface than in the subsurface region.

In this study, we have prepared a variety of Pd–Au surfaces by annealing the Pd/Au(111) surface to various temperatures in the absence (UHV) and presence of oxygen (1×10^{-6} Torr of O_2). These annealed Pd/Au(111) surfaces were characterized and tested in a fashion similar to the approach employed in our previous study.[52] The influence of annealing in oxygen on atomic structure and catalytic activity of Pd–Au bimetallic surfaces was investigated by comparing the physicochemical and catalytic properties of Pd–Au surfaces that were annealed in an O_2 environment *versus* under UHV conditions. The composition of the near-surface region of annealed Pd/Au(111) surfaces was analyzed *via* Auger electron spectroscopy (AES). The effect of surface oxygen coverage on total system energy and surface Pd coverage of the 1 ML Pd/Au(111) surface was simulated using Basin hopping (BH) methods.[53] The surface structures of UHV-annealed and oxygen-annealed Pd–Au surfaces were further investigated by reflection–absorption infrared spectroscopy using CO as a probe molecule (CO-RAIRS). King–Wells measurements and temperature-programmed desorption (TPD) were conducted to study the interactions of oxygen with annealed Pd/Au(111) surfaces. Finally, the catalytic activities for CO oxidation on UHV-annealed and oxygen-annealed Pd/Au(111) surfaces were compared *via* reactive molecular beam scattering (RMBS) experiments.

2. Experimental and computational methods

2.1 Model catalyst experiments

All experiments in this study were performed in an UHV chamber that has been described in detail previously.[54,55] Briefly, the chamber is equipped with an Auger electron spectrometer (Physical Electronics 10-500), a quadrupole mass spectrometer (Extrel C-50), a Fourier transform infrared spectrometer (Bruker Tensor 27) combined with a mercury–cadmium–telluride (MCT) detector (Infrared Associates), as well as nozzles and apertures for generating two separate molecular beams.

The Au(111) single-crystal sample is a circular disk (Princeton Scientific, 12 mm in diameter $\times$ 2 mm thick) held in place by a Mo wire fitted around a groove cut into the side of the sample. This wire is also used to resistively heat the sample and to provide thermal contact between the sample and a liquid nitrogen bath for cooling. The temperature of the sample was measured with a K-type (alumel–chromel) thermocouple placed into a small hole in the edge of the disk-shaped sample. The Au(111) surface was periodically cleaned by Ar ion bombardment (2 keV), carried out at room temperature, followed by an anneal to 800 K. The cleanliness of the surface was verified by AES with a beam energy of 3 keV and emission current of 1.5 mA.

Pd–Au bimetallic model surfaces were prepared by depositing 1.5 monolayer (ML) of Pd atoms from a homemade thermal evaporator onto the Au(111) surface at 77 K followed by annealing in either UHV or in an ambient of O_2 at 1×10^{-6} Torr to a specified temperature for 10 min.[52,56–58] The growth of the Pd overlayer on the Au(111) surface at 77 K has been suggested to obey a layer-by-layer mechanism.[57] Upon annealing in UHV, some of the surface Pd atoms can diffuse into the bulk of the Au(111) sample, forming a Pd–Au alloy at the surface.[7,36,40] As the annealing temperature is increased, the surface Pd morphology is transformed from a mixture of isolated and contiguous sites to a surface containing only isolated Pd sites.[7] The annealed Pd/Au(111) surface displays a relatively high degree of heterogeneity as compared to that of the Pd(111) surface.[52,57] The deposition rate of Pd was calibrated with a quartz crystal microbalance (QCM) controller (Maxtek Inc.) assuming a thickness of 1 ML Pd equals 0.274 nm.

CO-RAIRS was used to characterize the structure of annealed Pd/Au(111) surfaces.[52,56,57] The Pd–Au surface was first heated to 500 K at 1 K s^{-1} to desorb any surface contaminants such as CO. After the sample had cooled to 77 K, an IR background scan was taken. A saturation coverage of CO was then delivered by a molecular beam of CO with the sample held at 77 K. The IR spectrum of saturated CO adsorbed on the surface was taken at 77 K. All spectra were averaged from 512 scans with a resolution of 4 cm^{-1}.

The adsorption of oxygen molecules on Pd–Au surfaces was investigated by King–Wells measurements.[52,59–62] A neat O_2 molecular beam with a translational energy of $\sim$0.1 eV was first impinged on the stainless steel inert flag to establish a baseline. The beam was then impinged on the annealed Pd/Au(111) surface at a surface temperature of 77 K. The O_2 mass signal (m/z^+ = 32) was monitored by quadrupole mass spectrometry (QMS) during these King–Wells measurements.

For O_2-TPD and CO-RMBS experiments, the Pd–Au bimetallic surface was generated by depositing 1.5 ML Pd atoms on the Au(111) surface followed by annealing to 500 K for 10 min in UHV or an oxygen ambient. In O_2-TPD measurements, oxygen was dosed by impinging an O_2 beam on the Pd–Au surface at 77 K until its saturation. The surface was then heated at a rate of 1 K s^{-1} while m/z^+ = 32 (O_2) was monitored by QMS. For CO-RMBS experiments, the Pd–Au surface was first saturated

This journal is © the Owner Societies 2015

Phys. Chem. Chem. Phys., 2015, **17**, 20588–20596 | **20589**

with oxygen at 77 K by backfilling the chamber with 1 langmuir (L; 1 L = 1 × 10^{-6} Torr s) of O_2 through a leak valve.[52] The oxygen-precovered Pd–Au surface was then heated to 250 K prior to CO beam impingement. QMS signals of m/z^+ = 32 (O_2), 44 (CO_2) and 28 (CO) were monitored simultaneously during CO-RMBS experiments.

2.2 Basin hopping simulations

Basin hopping simulations were used to study the reorganization process of a Pd/Au(111) slab. The Pd/Au(111) slab was modeled as a five-layer 4 × 4 Au(111) slab with the bottom two layers fixed and the top layer initially replaced by a monolayer of Pd atoms. BH simulations with 200 trials were conducted on Pd/Au(111) slabs with various coverages of surface oxygen (θ_O = 0, 0.25 and 0.5 ML) at the temperature of 500 K. For each BH trial, one Pd atom was randomly selected to swap with one of its nearest-neighbor Au atoms. The acceptance probability (π) of each trial step was calculated by (eqn (1))

$$\pi = \min\left[1, \exp\left(-\frac{E_i - E_{i-1}}{kT}\right)\right] \tag{1}$$

in which E_{i-1} and E_i are the energies of DFT optimized structures (in eV) before and after the ith swapping trial step, k is the Boltzmann constant (8.617 × 10^{-5} eV K^{-1}) and T is the absolute temperature (in K).

All DFT calculations were performed with the Vienna *ab initio* simulation package.[63–66] The interaction between the ionic core and the valence electrons was described by the project augmented wave method,[67] and the valence electrons were described with a plane-wave basis up to an energy cutoff of 220 eV.[68,69] The exchange correlation contribution to the total energy functional was determined using the Perdew–Burke–Ernzerhof (PBE) generalized gradient approximation functional.[70] The Brillouin zone was sampled using a 2 × 2 × 1 Monkhorst–Pack k-point mesh.[71] The convergence criteria for the electronic structure and the atomic geometry were 10^{-4} eV and 0.05 eV Å^{-1}, respectively. A vacuum gap of 12 Å in the z-direction was used to avoid interactions from periodic images. Notably, values for the above computational parameters were chosen as a compromise of computational cost and proper physics.

3. Results and discussion

3.1 AES characterization of Pd/Au(111) surfaces

We analyzed the composition in the near-surface region of annealed Pd/Au(111) surfaces by AES. Fig. 1a and b show the AES spectra of the as-prepared Pd/Au(111) surface and those after annealing the surface to each specific temperature (*i.e.*, 500, 550 and 600 K) in UHV and 1 × 10^{-6} Torr of O_2, respectively.

It is noted that the oxygen-annealed Pd/Au(111) surface typically showed a small oxygen signal at ~510 eV in the AES spectrum immediately after annealing in oxygen ambient (Fig. S1 of ESI†). This oxygen signal was removed by simply heating the surface to 500 K (Fig. S1 of ESI†) to yield the oxygen-free AES spectra as shown in Fig. 1b. We speculate that the presence of an oxygen signal on the oxygen-annealed surface was due to adsorption of
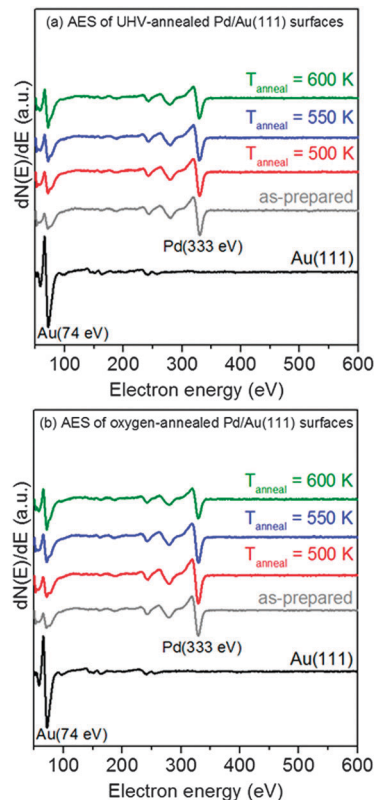

Fig. 1 AES spectra of as-prepared 1.5 ML Pd/Au(111) surface and those after annealing the surface to a specific temperature in (a) UHV and (b) 1 × 10^{-6} Torr of O_2.

background oxygen during sample cooling rather than formation of stable oxides on the Pd–Au surface. The adsorbed oxygen was weakly bound to the surface as indicated by desorption after mild heating. This weak binding suggests that oxygen species adsorbed on the surface are mainly in the molecular state as dissociated oxygen atoms recombine and desorb from the Pd–Au surface at the higher temperature of ~750 K.[72]

The thermal stability of the Pd film deposited on the Au(111) surface in UHV has been thoroughly investigated.[36,40,56] Upon annealing under UHV conditions, alloying occurs (*i.e.*, Pd atoms from the topmost layer diffuse into the subsurface of the Au(111) sample), which causes an increase in the Au LEISS signal intensity.[36] As shown in Fig. 1, intensification of the Au AES signal intensity and attenuation of the Pd AES signal intensity were both observed when the Pd/Au(111) surface was annealed in either UHV or an oxygen ambient. These observations suggest that annealing the Pd/Au(111) surface in oxygen ambient also results in the interdiffusion of surface Pd atoms into the Au(111) sample, the same phenomenon observed in the process of annealing in UHV.[36,40,56]

To further examine the influence of oxygen on the relative composition of Pd/Au(111) surfaces, the Pd(333 eV)/Au(74 eV) AES peak-to-peak ratios on the as-prepared surfaces and those annealed in UHV and oxygen were computed, as shown in Fig. 2.

With an annealing temperature of 500 K, the Pd/Au AES ratio on the oxygen-annealed Pd/Au(111) surface was significantly
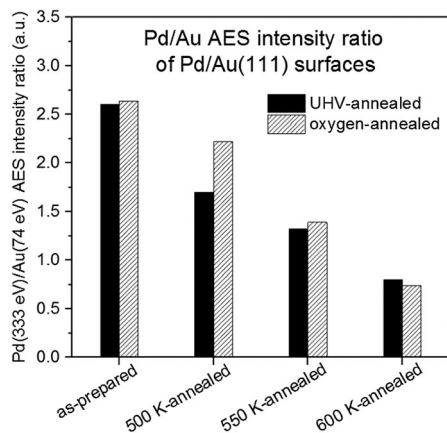
Fig. 2 Pd(333 eV)/Au(74 eV) AES intensity ratio of as-prepared and annealed 1.5 ML Pd/Au(111) bimetallic surfaces in Fig. 1.

higher than that on the UHV-annealed surface, which suggests that the presence of oxygen can inhibit the diffusion of surface Pd atoms into the Au(111) subsurface. When Pd/Au(111) surfaces were annealed at higher temperatures (*i.e.*, 550 and 600 K), the influence of adsorbed oxygen on the Pd/Au AES ratio became insignificant. We note that AES can detect not only the topmost layer of the surface but also the atoms in the near-surface region (the mean free path of electrons with energies between 10 and 1000 eV is of the order of a few atomic layers[73]). Accordingly, some Pd and Au atoms in the near-surface region that are not surface-accessible may also contribute to AES signals[46] on the annealed Pd/Au(111) surfaces.

3.2 Basin hopping simulations of Pd/Au(111) surfaces

The influence of surface oxygen coverages on the total system energy and surface Pd coverage (θ_{Pd}) of the 1 ML Pd/Au(111) surface was investigated by Basin hopping simulations. The simulation results and top views for initial and final structures are depicted in Fig. 3.

When oxygen atoms are absent from the surface ($\theta_O = 0$ ML), the mixing of surface Pd atoms into the Au(111) subsurface is energetically favorable and the surface Pd coverage decreases sharply as the simulation progresses. These results are consistent with our AES observations (Fig. 1 and 2) and previous studies using AES and LEISS characterizations[36] and STM imaging.[48,49] For surfaces partially covered with oxygen atoms, the total system energy does not decrease as significantly during the simulation process. After 200 swapping steps, the decreases in total system energy are ~ 7.2, 2.8 and 0.3 eV for surfaces with oxygen coverage of 0, 0.25 and 0.5 ML, respectively. These results suggest that the presence of surface oxygen atoms can stabilize the Pd/Au(111) system and the system is more energetically stable when more oxygen atoms are present on the surface.

Our Basin hopping simulations also show that the surface Pd coverage decreases more quickly in terms of number of
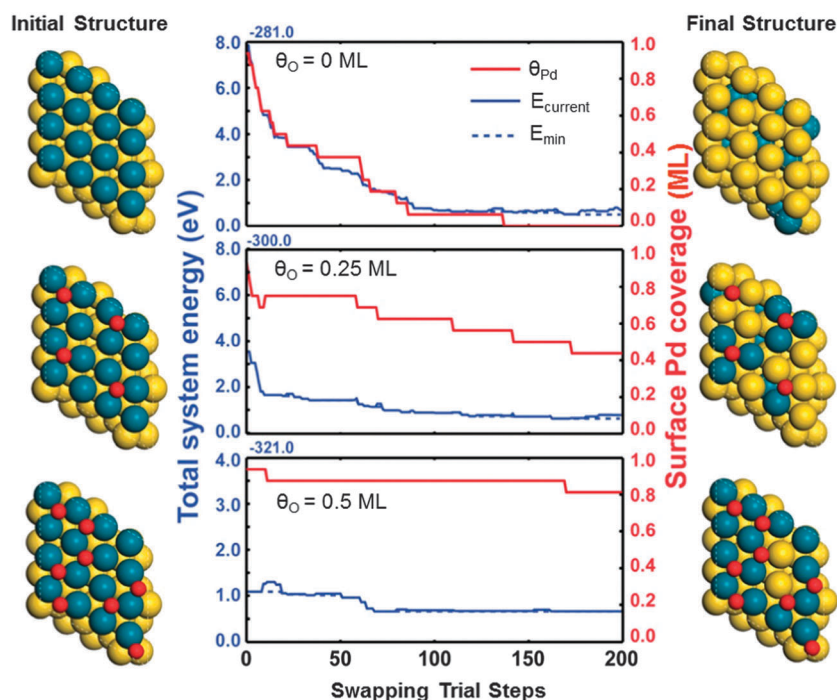

Fig. 3 Basin hopping simulations for the total system energy and surface Pd coverage of the 1 ML Pd/Au(111) surface in the absence and presence of surface oxygen atoms. For convenience of comparison, the energy for surfaces with oxygen coverage (θ_O) of 0, 0.25 and 1 ML are referenced to −281, −300 and −321 eV, respectively. Blue solid and dashed lines represent the energy for current structure ($E_{current}$) and lowest energy visited so far (E_{min}), respectively. Red solid lines represent the surface Pd coverage. The top views for initial and final structures are included on left and right sides, respectively.

This journal is © the Owner Societies 2015

Phys. Chem. Chem. Phys., 2015, **17**, 20588–20596 | **20591**

swapping steps on the surface lacking oxygen than on the surfaces containing oxygen. The surface Pd coverage on the oxygen-free surface (θ_O = 0 ML) decreases to zero after 135 swapping steps, while the surface Pd coverages only decrease to 0.43 and 0.8 ML after 200 swapping steps on the oxygen-covered surfaces with θ_O = 0.25 and 0.5 ML, respectively. These simulation results suggest that oxygen atoms on the Pd/Au(111) can prevent the interdiffusion of Pd atoms into the Au slab, which supports our earlier interpretation from AES spectra (Fig. 1 and 2) that surface oxygen atoms can inhibit the diffusion of surface Pd atoms into the Au(111) subsurface. These observations are also conceptually consistent with previous DFT studies,[50,51] in which the effect of oxygen on the segregation energy for Pd–Au surfaces was investigated using Pd monomer–Au(111) models.

The inhibition effect on Pd interdiffusion due to surface oxygen atoms likely results from the different strength between the O–Pd bond and the O–Au bond; because O binds to Pd more strongly than to Au, the swapping between surface Pd that bonds with oxygen and subsurface Au requires extra energy to overcome the energy difference between O–Pd and O–Au interactions. It is also worth noting that in the real case, the surface oxygen atoms that bond with Pd atoms could recombinatively desorb from the Pd–Au surface after Pd atoms are exchanged by Au atoms. This possible oxygen desorption was not included in our simulations in this study (it would be expected to further decrease the surface Pd coverage if oxygen desorption had been considered as a possibility).

3.3 CO-RAIRS characterization of Pd/Au(111) surfaces

The Pd/Au(111) surfaces annealed in UHV and oxygen were further characterized by CO-RAIRS. CO-RAIRS has long been used to study the properties and structures of model catalyst surfaces.[74,75] Information regarding the adsorption sites and surface morphology can be inferred from the observed CO stretching frequencies (ν_{CO}) as a result of varying degrees of π-antibonding back-donation from the surface electrons.[74,75]

Fig. 4 shows the RAIRS spectra of saturated CO on Au(111) and UHV-annealed and oxygen-annealed 1.5 ML Pd/Au(111) surfaces. According to previously reported literature,[42,43,76] the assignment for the IR features of CO adsorbed on Pd–Au model surfaces has been established as follows:[77] ν_{CO} at 1900–2000, 2160–2085 and >2100 cm^{-1} corresponds to bridged CO on contiguous Pd sites, atop CO on isolated Pd sites, and atop CO on Au sites, respectively. As shown in Fig. 4a, the Pd/Au(111) surface annealed in UHV at 500 K displayed two main IR bands at ~2087 and 1965 cm^{-1}, which can be attributed to CO adsorbed on isolated and contiguous Pd sites, respectively. These two IR bands shifted to higher frequencies at ~2090 and 1976 cm^{-1} on the Pd/Au(111) surface annealed in oxygen at 500 K (Fig. 4b). When the annealing temperature was increased, the intensity of the IR feature due to contiguous Pd sites attenuated and that due to isolated Pd sites intensified on both UHV-annealed and oxygen-annealed surfaces. For the same annealing temperature, the IR feature associated with contiguous Pd sites was consistently larger for the oxygen-annealed surfaces than for the UHV-annealed surfaces. These observations suggest
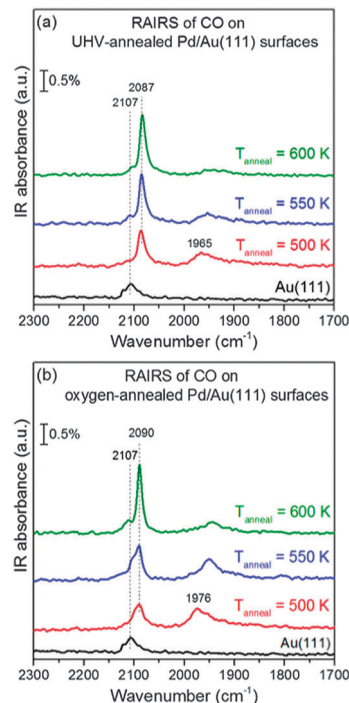

Fig. 4 RAIRS spectra of saturated CO on Au(111) and 1.5 ML Pd/Au(111) surfaces annealed in (a) UHV and (b) 1×10^{-6} Torr of O$_2$ at various temperatures. These spectra were taken at a surface temperature of 77 K.

that a higher number of contiguous Pd atoms are present on oxygen-annealed surfaces in comparison to that on UHV-annealed surfaces.

It is noted that although CO-RAIRS can provide qualitative information such as surface morphology and adsorption sites of Pd–Au model surfaces, quantitative analysis using CO-RAIRS is quite difficult when contiguous Pd sites are present on the surface,[58] likely due to the vibrational coupling effect that attenuates the IR intensity at high surface CO coverages.[43]

3.4 Oxygen adsorption and desorption on Pd/Au(111) surfaces

As mentioned earlier, Pd–Au catalysts have displayed promising performance in a number of catalytic reactions involving oxygen as a reactant.[3–11,23–28] Accordingly, it is of interest to investigate the interaction of oxygen with the annealed Pd/Au(111) surfaces in this study. King–Wells measurements have been employed to study the adsorption of oxygen molecules on UHV-annealed Pd/Au(111) surfaces.[52] By analyzing the O$_2$ QMS signals from the inert flag and sample surface during the King–Wells measurement, (semi-)quantitative information such as the initial sticking probability and total uptake of oxygen molecules on the surface can be determined.[52]

Fig. 5 shows the O$_2$ QMS signal during a series of King–Wells measurements in which an O$_2$ molecular beam was impinged onto annealed 1.5 ML Pd/Au(111) surfaces. In these measurements, the O$_2$ beam was first impinged onto the inert flag for 5 s (from 10 to 15 s) to establish a baseline signal (all O$_2$ molecules scattered from the inert flag with negligible adsorption), and then impinged onto the annealed Pd/Au(111) surfaces that
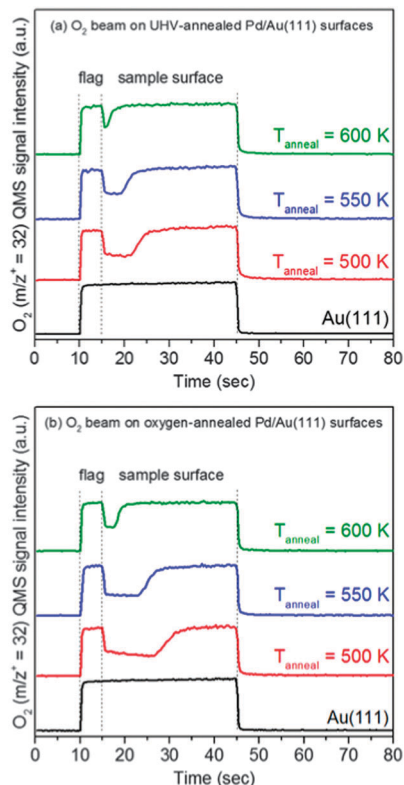
Fig. 5 O_2 (m/z^+ = 32) QMS signals detected during King–Wells measurements. The 1.5 ML Pd/Au(111) surfaces were annealed to the specified temperature in (a) UHV and (b) 1×10^{-6} Torr of O_2. For these measurements, an O_2 beam was impinged on the surface at 77 K.

were held at 77 K for 30 s (from 15 to 45 s). The same measurements were carried out on the clean (Pd-free) Au(111) surface for comparison.

A constant O_2 QMS signal was detected when the O_2 beam was impinged on the inert flag and Au(111) surface, indicating that oxygen was not adsorbed on the Au(111) surface under this condition. The intensity of the O_2 QMS signal upon impingement of the beam onto each annealed Pd/Au(111) surface was initially lower than that from impingement onto the inert flag due to the adsorption of oxygen on the surface. We attributed this observed adsorption to be molecular in nature[52] since oxygen molecularly adsorbs on the Pd(111) surface at 80 K,[78] and the dissociation of oxygen admolecules occurs at higher temperatures between $\sim$180–200 K.[78–80] The initial sticking probability for oxygen molecules on each surface can be estimated from the O_2 QMS signal intensities from the inert flag and sample surface (Fig. S2 of ESI†). The initial sticking probability for the oxygen-annealed Pd/Au(111) surfaces is $\sim$0.48–0.52, which is slightly higher than that for the UHV-annealed surface ($\sim$0.43–0.45). It has been reported that the presence of contiguous Pd sites on Pd–Au surfaces is crucial for adsorption of oxygen molecules and that surfaces with only isolated Pd sites do not readily uptake O_2.[52] Accordingly, we speculate that the higher initial sticking probability observed here is due to a higher number of contiguous Pd sites present on oxygen-annealed Pd/Au(111) surfaces as compared to those on UHV-annealed surfaces.
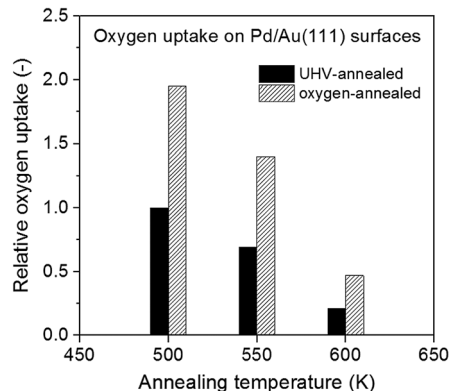

Fig. 6 The O_2 uptake (relative to that on the Pd/Au(111) surface annealed in UHV at 500 K) on annealed Pd/Au(111) surfaces during King–Wells measurements (Fig. 5).

The oxygen uptake on each surface during the King–Wells measurements can be computed using the O_2 QMS signals from the inert flag and sample surface (Fig. S3 of ESI†). The oxygen uptake on each surface is expressed as the relative oxygen uptake, which is relative to the oxygen uptake on the Pd/Au(111) surface annealed in UHV at 500 K (Fig. 6).

As expected, when the annealing temperature was increased, the oxygen uptakes on UHV-annealed and oxygen-annealed surfaces were both decreased due to diffusion of surface Pd atoms into the Au(111) subsurface during annealing. For UHV-annealed surfaces, the oxygen uptake on the surface annealed at 500 K decreased by 31% and 79% when surfaces were annealed at 550 and 600 K, respectively. The decrease in oxygen uptake was found to be smaller on oxygen-annealed surfaces; the oxygen uptake on the surface annealed at 500 K in an oxygen ambient decreased by 23% and 69% when annealing at 550 at 600 K, respectively. With the same annealing temperature, the oxygen uptake was consistently larger on oxygen-annealed surfaces than that on UHV-annealed surfaces. Since the oxygen adsorption sites on Pd/Au(111) surfaces consist of contiguous Pd atoms,[52] these observations support that oxygen-annealed Pd/Au(111) surfaces contain more contiguous Pd atoms than UHV-annealed Pd/Au(111) surfaces, which are consistent with CO-RAIRS spectra (Fig. 4). It is noted that despite their similar Pd/Au AES ratios (Fig. 2), the Pd/Au(111) surfaces annealed in UHV and oxygen at temperatures of 550 and 600 K display a significant difference in their oxygen uptake. This is explained as due to some of the Pd atoms residing in the subsurface region which will be detected by AES but unable to adsorb molecular oxygen. These results provide strong evidence that the presence of oxygen can keep Pd atoms on the topmost layer on Pd/Au(111) surfaces during annealing.

Fig. 7 shows the TPD spectra of saturated O_2 from UHV-annealed and oxygen-annealed Pd/Au(111) surfaces. The Pd–Au surfaces were generated by depositing 1.5 ML Pd on the Au(111) surface at 77 K followed by annealing at 500 K in either UHV or 1×10^{-6} Torr of O_2. The surfaces were saturated with oxygen at 77 K by impinging a molecular beam of O_2 onto the surface prior to heating. To more clearly visualize desorption features, the O_2-TPD spectra
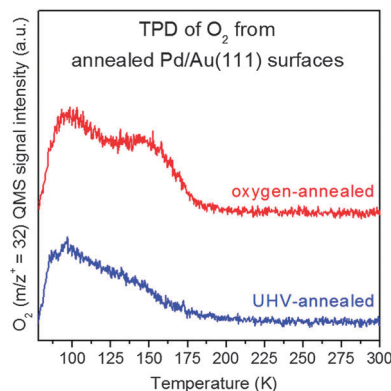
This journal is © the Owner Societies 2015

Phys. Chem. Chem. Phys., 2015, 17, 20588–20596 | 20593

Fig. 7 O_2 ($m/z^+ = 32$) QMS signals detected during O_2-TPD measurements. The 1.5 ML Pd/Au(111) surfaces were annealed at 500 K in UHV and 1×10^{-6} Torr of O_2. A saturation coverage of oxygen was dosed by impingement of O_2 beam at 77 K. The heating rate is 1 K s^{-1}.

were plotted within the temperature range between 77 and 300 K (no oxygen desorption was observed at temperatures greater than 300 K).

The interaction of oxygen has been studied on the UHV-annealed Pd/Au(111) surfaces by O_2-TPD.[52] According to the desorption temperature, it was shown that with the exposure to O_2 at 77 K the oxygen admolecules on the UHV-annealed Pd/Au(111) surface desorbed molecularly ($< \sim 220$ K) without detectable dissociation upon heating.[52] In Fig. 7, the oxygen desorption peak from the UHV-annealed and oxygen-annealed Pd/Au(111) surfaces both ended at ~ 200 K, which resulted from the desorption of molecularly adsorbed oxygen. The UHV-annealed surface displayed a broad O_2-TPD feature with a peak at ~ 97 K and a small shoulder at 140 K. This broad feature has been attributed to the higher degree of surface heterogeneity compared to that of the Pd(111) surface.[52] It is noted that compared to the UHV-annealed surface, the shoulder of desorption peak (at ~ 148 K) became much more significant on the oxygen-annealed surface. High-resolution electron energy loss spectroscopy (HREELS) showed[79,80] that oxygen molecules chemisorbed on the Pd(111) surface exist in three molecular states (one superoxo- and two peroxo-like species) with different vibrational frequencies of O–O stretching due to varying degrees of electron transfer from the surface into the oxygen molecule. Corresponding to these molecular states, three desorption features with peak temperatures of ~ 125, 150 and 200 K were observed.[78] We speculate that oxygen admolecules desorbed at ~ 148 K may exist in a different molecular state that bind more strongly to the surface than those desorbed at ~ 97 K (Fig. 7). These observations also suggest that the oxygen admolecules interact more strongly with oxygen-annealed surfaces than with UHV-annealed surfaces.

Weaver and co-workers[81] have studied the O_2-TPD from the PdO(101) surface. In their O_2-TPD spectra, two main TPD peaks centered at 117 and 227 K as well as smaller features at 275 and 315 K were observed due to desorption of molecularly chemisorbed O_2.[81] The absence of a O_2-TPD feature at temperatures above 200 K in Fig. 7 suggests that no oxide such as PdO was

formed after annealing the Pd/Au(111) surface in oxygen ambient, which is consistent with our observations from AES spectra (Fig. S1 of ESI†). It is noted that while PdO formation was not observed on the annealed Pd/Au(111) surface under the high vacuum conditions (10^{-6} Torr of O_2) employed in this study, the formation of PdO has been reported on the supported Pd–Au catalysts that were calcined in air at atmospheric pressure.[5,20,26]

3.5 Reaction of oxygen and CO on Pd/Au(111) surfaces

CO oxidation was employed to assess the catalytic activities of UHV-annealed and oxygen-annealed Pd/Au(111) surfaces by monitoring CO_2 production during CO-RMBS. As shown in Fig. 8, CO-RMBS experiments were conducted by impinging a molecular beam of CO onto the inert flag for 5 s (from 10 to 15 s), and then onto the oxygen-precovered Pd–Au surface for 60 s (from 15 to 75 s). For these measurements, the Pd–Au surface was generated by depositing 1.5 ML Pd onto the Au(111) surface at 77 K followed by annealing at 500 K in either UHV or 1×10^{-6} Torr of O_2. The surface was presaturated with molecular oxygen at 77 K and then heated to 250 K prior to CO beam impingement.

Upon CO beam impingement at 250 K, CO_2 evolution was both detected from both UHV-annealed and oxygen-annealed Pd/Au(111) surfaces. A time delay for emergence of CO_2 signals has been attributed to the site blocking from oxygen and hydrogen impurities (from adsorption of background gas that is intrinsically present in our UHV chamber) on the Pd–Au surface.[52] The CO_2 peak observed from the oxygen-annealed Pd/Au(111) surface was larger than that from the UHV-annealed surface, indicative of a higher yield of CO_2 on the oxygen-annealed surface. These observations demonstrate that the oxygen-annealed Pd/Au(111) surface is more active for CO oxidation than the UHV-annealed Pd/Au(111) surface.

In a previous study using CO-RMBS,[52] we have shown that CO_2 was produced on the Pd/Au(111) surface *via* the reaction of CO with atomic oxygen (dissociative pathway) rather than molecular oxygen (associative pathway). An associative mechanism was not observed, which is likely due to facile CO-induced O_2 desorption.[52] The CO_2 production from the annealed Pd/Au(111)
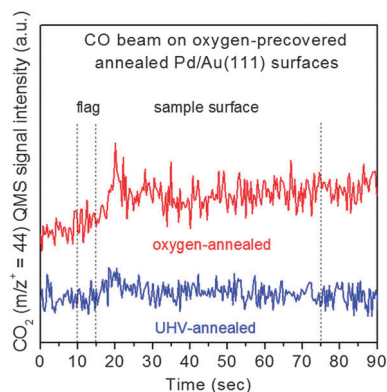

Fig. 8 CO_2 ($m/z^+ = 44$) QMS signals detected during CO-RMBS experiments. The 1.5 ML Pd/Au(111) surfaces were annealed at 500 K in UHV and 1×10^{-6} Torr of O_2. The surface was presaturated with molecular oxygen at 77 K and then heated to 250 K prior to CO beam impingement.

surface at 250 K in Fig. 8 is due to the reaction of CO with atomic oxygen as the desorption of molecular oxygen had completed at a temperature of ~ 200 K (Fig. 7). Accordingly, the higher activity for CO_2 production suggests that the dissociation of oxygen admolecules into oxygen adatoms is more facile on the oxygen-annealed surface than on the UHV-annealed surface. The relative ease of dissociation of oxygen admolecules could originate from the stronger interaction between O_2 and the oxygen-annealed Pd/Au(111) surface as suggested from O_2-TPD spectra (Fig. 7).

4. Conclusions

We have conducted a model catalyst study that combines experimental and theoretical methods to investigate the effect of annealing in oxygen on the alloy structure and composition of Pd–Au bimetallic surfaces. Results based on AES, Basin hopping simulations and CO-RAIRS show that the presence of oxygen can inhibit the diffusion of surface Pd atoms into the Au(111) subsurface during annealing, resulting in a higher amount of Pd atoms present on the surface. Compared to the UHV-annealed Pd/Au(111) surface, the oxygen-annealed Pd/Au(111) surface exhibited a higher oxygen uptake during King–Wells measurements and stronger interactions with oxygen molecules in O_2-TPD experiments. CO-RMBS tests reveal that the oxygen-annealed Pd/Au(111) surface was more active than the UHV-annealed Pd/Au(111) surface for catalyzing CO oxidation to form CO_2. This enhanced activity on the oxygen-annealed surface is likely due to the higher oxygen uptake and a relatively more facile dissociation of oxygen admolecules. These results may enhance the fundamental understanding of Pd–Au alloy formation during calcination, and in turn aid the rational design of improved Pd–Au catalysts.

Acknowledgements

References

1 J. G. Chen, C. A. Menning and M. B. Zellner, *Surf. Sci. Rep.*, 2008, **63**, 201.
2 F. Gao and D. W. Goodman, *Chem. Soc. Rev.*, 2012, **41**, 8009.
3 F. Gao, Y. L. Wang and D. W. Goodman, *J. Phys. Chem. C*, 2010, **114**, 4036.
4 J. Xu, T. White, P. Li, C. H. He, J. G. Yu, W. K. Yuan and Y. F. Han, *J. Am. Chem. Soc.*, 2010, **132**, 10398.
5 Z. H. Suo, C. Y. Ma, M. S. Jin, T. He and L. D. An, *Catal. Commun.*, 2008, **9**, 2187.
6 Y. F. Han, J. H. Wang, D. Kumar, Z. Yan and D. W. Goodman, *J. Catal.*, 2005, **232**, 467.
7 M. S. Chen, D. Kumar, C. W. Yi and D. W. Goodman, *Science*, 2005, **310**, 291.
8 D. I. Enache, J. K. Edwards, P. Landon, B. Solsona-Espriu, A. F. Carley, A. A. Herzing, M. Watanabe, C. J. Kiely, D. W. Knight and G. J. Hutchings, *Science*, 2006, **311**, 362.
9 D. Wang, A. Villa, F. Porta, D. S. Su and L. Prati, *Chem. Commun.*, 2006, 1956.
10 N. Dimitratos, J. A. Lopez-Sanchez, J. M. Anthonykutty, G. Brett, A. F. Carley, R. C. Tiruvalam, A. A. Herzing, C. J. Kiely, D. W. Knight and G. J. Hutchings, *Phys. Chem. Chem. Phys.*, 2009, **11**, 4952.
11 A. Villa, D. Wang, D. S. Su, G. M. Veith and L. Prati, *Phys. Chem. Chem. Phys.*, 2010, **12**, 2183.
12 A. Hugon, L. Delannoy, J.-M. Krafft and C. Louis, *J. Phys. Chem. C*, 2010, **114**, 10823.
13 R. X. Liu, Y. C. Yu, K. Yoshida, G. M. Li, H. X. Jiang, M. H. Zhang, F. Y. Zhao, S. Fujita and M. Arai, *J. Catal.*, 2010, **269**, 191.
14 X. Yang, D. Chen, S. Liao, H. Song, Y. Li, Z. Fu and Y. Su, *J. Catal.*, 2012, **291**, 36.
15 N. El Kolli, L. Delannoy and C. Louis, *J. Catal.*, 2013, **297**, 79.
16 M. O. Nutt, J. B. Hughes and M. S. Wong, *Environ. Sci. Technol.*, 2005, **39**, 1346.
17 Y. L. Fang, K. N. Heck, P. J. J. Alvarez and M. S. Wong, *ACS Catal.*, 2011, **1**, 128.
18 Y. L. Fang, J. T. Miller, N. Guo, K. N. Heck, P. J. J. Alvarez and M. S. Wong, *Catal. Today*, 2011, **160**, 96.
19 A. M. Venezia, V. La Parola, G. Deganello, B. Pawelec and J. L. G. Fierro, *J. Catal.*, 2003, **215**, 317.
20 Z. Suo, C. Ma, W. Liao, M. Jin and H. Lv, *Fuel Process. Technol.*, 2011, **92**, 1549.
21 X. C. Zhou, Y. J. Huang, W. Xing, C. P. Liu, J. H. Liao and T. H. Lu, *Chem. Commun.*, 2008, 3540.
22 O. Metin, X. L. Sun and S. H. Sun, *Nanoscale*, 2013, **5**, 910.
23 P. Landon, P. J. Collier, A. F. Carley, D. Chadwick, A. J. Papworth, A. Burrows, C. J. Kiely and G. J. Hutchings, *Phys. Chem. Chem. Phys.*, 2003, **5**, 1917.
24 J. K. Edwards, B. Solsona, N. N. Edwin, A. F. Carley, A. A. Herzing, C. J. Kiely and G. J. Hutchings, *Science*, 2009, **323**, 1037.
25 J. K. Edwards, A. F. Carley, A. A. Herzing, C. J. Kiely and G. J. Hutchings, *Faraday Discuss.*, 2008, **138**, 225.
26 J. K. Edwards, J. Pritchard, M. Piccinini, G. Shaw, Q. He, A. F. Carley, C. J. Kiely and G. J. Hutchings, *J. Catal.*, 2012, **292**, 227.
27 J. K. Edwards and G. J. Hutchings, *Angew. Chem., Int. Ed.*, 2008, **47**, 9192.
28 J. K. Edwards, S. J. Freakley, A. F. Carley, C. J. Kiely and G. J. Hutchings, *Acc. Chem. Res.*, 2014, **47**, 845.
29 A. Cybula, J. B. Priebe, M. M. Pohl, J. W. Sobczak, M. Schneider, A. Zielhiska-Jurek, A. Bruckner and A. Zaleska, *Appl. Catal., B*, 2014, **152**, 202.
30 C. T. Campbell, *Annu. Rev. Phys. Chem.*, 1990, **41**, 775.
31 G. A. Somorjai, *Chem. Rev.*, 1996, **96**, 1223.
32 J. F. Weaver, A. F. Carlsson and R. J. Madix, *Surf. Sci. Rep.*, 2003, **50**, 107.

This journal is © the Owner Societies 2015

Phys. Chem. Chem. Phys., 2015, **17**, 20588–20596 | **20595**

33 J. Libuda and H. J. Freund, *Surf. Sci. Rep.*, 2005, **57**, 157–298.

34 J. L. Gong, *Chem. Rev.*, 2012, **112**, 2987.

35 M. Pan, A. J. Brush, Z. D. Pozun, H. C. Ham, W.-Y. Yu, G. Henkelman, G. S. Hwang and C. B. Mullins, *Chem. Soc. Rev.*, 2013, **42**, 5002.

36 B. E. Koel, A. Sellidj and M. T. Paffett, *Phys. Rev. B: Condens. Matter Mater. Phys.*, 1992, **46**, 7846.

37 A. Sellidj and B. E. Koel, *Phys. Rev. B: Condens. Matter Mater. Phys.*, 1994, **49**, 8367.

38 R. M. Ormerod, C. J. Baddeley and R. M. Lambert, *Surf. Sci.*, 1991, **259**, L709.

39 C. J. Baddeley, C. J. Barnes, A. Wander, R. M. Ormerod, D. A. King and R. M. Lambert, *Surf. Sci.*, 1994, **314**, 1.

40 C. J. Baddeley, R. M. Ormerod, A. W. Stephenson and R. M. Lambert, *J. Phys. Chem.*, 1995, **99**, 5146.

41 C. J. Baddeley, M. Tikhov, C. Hardacre, J. R. Lomas and R. M. Lambert, *J. Phys. Chem.*, 1996, **100**, 2189.

42 C. W. Yi, K. Luo, T. Wei and D. W. Goodman, *J. Phys. Chem. B*, 2005, **109**, 18535.

43 T. Wei, J. Wang and D. W. Goodman, *J. Phys. Chem. C*, 2007, **111**, 8781.

44 L. Piccolo, A. Piednoir and J. C. Bertolini, *Surf. Sci.*, 2005, **592**, 169.

45 Z. Li, F. Gao, Y. Wang, F. Calaza, L. Burkholder and W. T. Tysoe, *Surf. Sci.*, 2007, **601**, 1898.

46 Z. J. Li, O. Furlong, F. Calaza, L. Burkholder, H. C. Poon, D. Saldin and W. T. Tysoe, *Surf. Sci.*, 2008, **602**, 1084.

47 H. L. Tierney, A. E. Baber, J. R. Kitchin and E. C. H. Sykes, *Phys. Rev. Lett.*, 2009, **103**, 246102.

48 A. E. Baber, H. L. Tierney and E. C. H. Sykes, *ACS Nano*, 2010, **4**, 1637.

49 A. E. Baber, H. L. Tierney, T. J. Lawton and E. C. H. Sykes, *ChemCatChem*, 2011, **3**, 607.

50 H. Guesmi, C. Louis and L. Delannoy, *Chem. Phys. Lett.*, 2011, **503**, 97.

51 A. Dhouib and H. Guesmi, *Chem. Phys. Lett.*, 2012, **521**, 98.

52 W.-Y. Yu, L. Zhang, G. M. Mullen, G. Henkelman and C. B. Mullins, *J. Phys. Chem. C*, 2015, **119**, 11754.

53 D. J. Wales and J. P. K. Doye, *J. Phys. Chem. A*, 1997, **101**, 5111.

54 D. W. Flaherty, N. T. Hahn, D. Ferrer, T. R. Engstrom, P. L. Tanaka and C. B. Mullins, *J. Phys. Chem. C*, 2009, **113**, 12742.

55 D. W. Flaherty, W.-Y. Yu, Z. D. Pozun, G. Henkelman and C. B. Mullins, *J. Catal.*, 2011, **282**, 278.

56 W.-Y. Yu, G. M. Mullen and C. B. Mullins, *J. Phys. Chem. C*, 2013, **117**, 19535.

57 W.-Y. Yu, G. M. Mullen and C. B. Mullins, *J. Phys. Chem. C*, 2014, **118**, 2129.

58 W.-Y. Yu, G. M. Mullen, D. W. Flaherty and C. B. Mullins, *J. Am. Chem. Soc.*, 2014, **136**, 11070.

59 D. A. King and M. G. Wells, *Proc. R. Soc. London, Ser. A*, 1974, **339**, 245.

60 M. C. Wheeler, D. C. Seets and C. B. Mullins, *J. Chem. Phys.*, 1996, **105**, 1572.

61 J. E. Davis, S. G. Karseboom, P. D. Nolan and C. B. Mullins, *J. Chem. Phys.*, 1996, **105**, 8362.

62 J. E. Davis, P. D. Nolan, S. G. Karseboom and C. B. Mullins, *J. Chem. Phys.*, 1997, **107**, 943.

63 G. Kresse and J. Hafner, *Phys. Rev. B: Condens. Matter Mater. Phys.*, 1993, **47**, 558.

64 G. Kresse and J. Hafner, *Phys. Rev. B: Condens. Matter Mater. Phys.*, 1994, **49**, 14251.

65 G. Kresse and J. Furthmuller, *Phys. Rev. B: Condens. Matter Mater. Phys.*, 1996, **54**, 11169.

66 G. Kresse and J. Furthmuller, *Comput. Mater. Sci.*, 1996, **6**, 15.

67 P. E. Blochl, *Phys. Rev. B: Condens. Matter Mater. Phys.*, 1994, **50**, 17953.

68 P. Hohenberg and W. Kohn, *Phys. Rev. B: Condens. Matter Mater. Phys.*, 1964, **136**, B864.

69 W. Kohn and L. J. Sham, *Phys. Rev.*, 1965, **140**, 1133.

70 J. P. Perdew, K. Burke and M. Ernzerhof, *Phys. Rev. Lett.*, 1996, **77**, 3865.

71 H. J. Monkhorst and J. D. Pack, *Phys. Rev. B: Solid State*, 1976, **13**, 5188.

72 Z. J. Li, F. Gao and W. T. Tysoe, *J. Phys. Chem. C*, 2010, **114**, 16909.

73 G. Ertl, J. Kuppers, *Low Energy Electrons and Surface Chemistry*, VCH, 1985, ch. 1, pp. 6–8.

74 M. Trenary, *Annu. Rev. Phys. Chem.*, 2000, **51**, 381.

75 E. L. Wilson and W. A. Brown, *J. Phys. Chem. C*, 2010, **114**, 6879.

76 K. Luo, T. Wei, C. W. Yi, S. Axnanda and A. W. Goodman, *J. Phys. Chem. B*, 2005, **109**, 23517.

77 F. Gao, Y. L. Wang and D. W. Goodman, *J. Am. Chem. Soc.*, 2009, **131**, 5734.

78 X. C. Guo, A. Hoffman and J. T. Yates, *J. Chem. Phys.*, 1989, **90**, 5787.

79 R. Imbihl and J. E. Demuth, *Surf. Sci.*, 1986, **173**, 395.

80 K. W. Kolasinski, F. Cemic and E. Hasselbrink, *Chem. Phys. Lett.*, 1994, **219**, 113.

81 J. A. Hinojosa, H. H. Kan and J. F. Weaver, *J. Phys. Chem. C*, 2008, **112**, 8324.